




Journal of Rehabilitation in Civil Engineering

Journal homepage: <https://civiljournal.semnan.ac.ir/>

## Experimental and FEM Analyses of RC Beams with Radius Corner Arch at Bottom Tension Face

Maryam H. Naser<sup>1</sup>; Fatimah H. Naser<sup>2,\*</sup> ; Ali Hameed Naser Almamoori<sup>3</sup>; Mohammed L. Hussien<sup>4</sup>

1. Department of Water Resources Management Engineering, College of Engineering, Al-Qasim Green University, Babylon 51013, Iraq

2. Department of Civil Engineering, College of Engineering, Al-Qasim Green University, Babylon 51013, Iraq

3. Department of Civil Engineering, College of Engineering, University of Kerbala, Kerbala, Iraq

4. Department of Medical Physics, College of Sciences, Al-Mustaqbal University, Babylon 51001, Iraq

\* Corresponding author: [fatimah\\_mamoori@wrec.uoqasim.edu.iq](mailto:fatimah_mamoori@wrec.uoqasim.edu.iq)

### ARTICLE INFO

#### Article history:

Received: 26 March 2023

Revised: 08 June 2023

Accepted: 05 July 2023

#### Keywords:

Nonlinear analysis;  
Reinforced concrete;  
Beam;  
Radius corner arch;  
Bottom tension face.

### ABSTRACT

The present study includes experimental and numerical investigations of the behavior and the load carrying capacity of RC two-hinged beams with radius corner arch at the bottom face subjected to static loading conditions. The experimental program included four specimens with the same volume of concrete and amount of steel reinforcement but, with a different span of the arch (1180 mm, 900 mm, 740 mm, and 600 mm). The goals were to evaluate the effect of a span of the arch and to find the optimum ratio of the arch length to beam span for the maximum load capacity as well as to validate the numerical results taken from the finite element model. From the results of this work, it was found that the best load carrying capacity for the beam with a radius corner arch is when the arch length/beam span ratio is equal (0.62). Also, the FEM result seems efficient and gives good accuracy through comparison with the experimental results.

E-ISSN: 2345-4423

© 2024 The Authors. Journal of Rehabilitation in Civil Engineering published by Semnan University Press.

This is an open access article under the CC-BY 4.0 license. (<https://creativecommons.org/licenses/by/4.0/>)

#### How to cite this article:

H. Naser, M., H. Naser, F., Hameed Naser Almamoori, A., & L. Hussien, M. (2024). Experimental and FEM Analyses of RC Beams with Radius Corner Arch at Bottom Tension Face. Journal of Rehabilitation in Civil Engineering, 12(2), 26-40. <https://doi.org/10.22075/jrce.2023.30269.1828>

## 1. Introduction

The arch is a structure that extends space and backings the structure and weight below it. Over the years, arches of different forms have been constructed for bridges, and buildings, as well as for monumental, historical, and cultural purposes. These have become architectural masterpieces gradually. It was a customary practice in ancient times to build arches for royal and heritage buildings[1] as shown in Fig. 1. In the olden days, bridges were built mainly using single arches lying in one plane at a single location. Not only arches have been built in single planes and at single locations but also in clusters lying in multiple planes. In modern times, arches are built using steel too. It is also common to construct arches in concrete. Reinforced concrete included many real and perceived characteristics compared to metal truss bridges. The utilization of concrete bridges offered durability and little maintenance in addition less dependent on (big steel) companies.

Also, the fundamental objective of the arches is to improve the load carrying capacity, which might originate from the hardening conduct because of membrane action, which urges scientists to consider the behavior of reinforced concrete arch beams. Alongside the new advancements in civil design, it could be considered the best system with less weight and high strength by redistributing material along structural beams which exemplified a structurally competitive solution in numerous utilizations of structural design, like buildings and bridges [2].



Fig. 1. Some examples of arch structures[3].

The literature studies indicated numerous experimental and theoretical research on the behavior of arched and non-prismatic beams. Where the non-prismatic and arched beam has been widely used in long-span bridges. In 1989 Alas, [4] solved one of the large problems in the analysis of beams with second moment varying along their length, is to find stiffness, the fixed end moments, and carry-over factors. Kaveh et al. [5] found that the use of non-prismatic beams in RC frames reduces the optimal economic costs and optimal CO2 emissions. To enhance the shear failure, Hans et al. [6] examined ten model supported RC beams (eight haunched and two prismatic). From the results, haunched beams have higher energy dissipation capacities and deformation than prismatic beams. Rojas [7] presented the mathematical model by the Simpson's rule applies for rectangular beams subjected to a uniformly distributed load of varied cross section for symmetric parabolic haunches. Additionally, a comparison was made between the suggested models and the tables that some authors have used. Nabbat [8] presented experimental and numerical investigations of the bending and shear behavior of non-prismatic RC beams strengthened by CFRP (bar or sheet). The results showed that the final load increased by (16% and 15%) for the flexural and shear behavior for beams, respectively. Jolly[9] presented a study to the structural behavior of reinforced concrete haunched beam in ANSYS and ETABS. Comparison of prismatic and reinforced concrete haunched beam in terms of displacement and stress intensity has been done by performing nonlinear static analysis in ANSYS. Naser et al.,[10] explain the nonlinear behavior of reinforced concrete haunched beams (RCHBs). This study aims to explore the structural reaction and strength capability of RCHBs exposure to two-point load for shear behavior by conducting nonlinear static analysis by ABAQUS. Then, the FE model was confirmed vs an

experimental work available in the literature, which demonstrated a strong agreement.

Elkersh et al.[11] present experimental investigation for three beams, one control beam with arched only and two beams with arched and with rectangular open, once in shear and another in flexure by using ANSYS program. The result showed that when the rectangular opening at the shear zone, the bearing capacity of the beam with arched opening decreases by about 5 % and the deflection decreases by 17 % compared to control beam. Many specialists provided experimental and analytical investigations of reinforced concrete arches under constant load on different cross-shapes with the special requirements such as Sfakianakis et al.[12], Al-Thabhwawi[13] and Hamza[14]. Ali and Kadhum [15] presented an accurate modeling strategy for the three-dimensional (3D) nonlinear finite element analysis of reinforced concrete (RC) columns. The concrete damaged plasticity (CDP) was used to model the nonlinear behavior of the concrete material in the compression and the tension. Through comparing the experimental data and numerical results, the effect of various parameters, such as the type of stress–strain relationships used for modeling the behavior of confined concrete and the type of element used to model the stirrups, were evaluated. Ibrahim et al.[16] investigated the elasto-plastic numerical modelling of reinforced concrete haunched beams under monotonic loading as optimization problems (limit load problem and minimum volume design). It was considered a validation of the numerical model on the reliance of the data obtained experimentally using the concrete damage plasticity (CDP) constitutive model in ABAQUS to represent the concrete behavior. Then, different optimization problems using MATLAB were executed

But the current study differs from what was previously studied, here the behavior of arc reinforced concrete beams in the face of lower

tension will be studied using high strength concrete (HSC). Accordingly, this study attempts to assess the change of arch length on the behavior of beams having the same amount of reinforcement and volume of concrete to obtain the optimum ratio for the maximum load capacity of arch length/beam span and to confirm the numerical findings obtained from the finite element model. Knowing that the distribution of stress in the beam with arched bottom would be quite different from that in an arched beam case because of the effect of the variable cross-section.

## **2. Experimental work**

### **2.1. Specimens description**

The experimental program contained four two-hinge beams including arched at the tension face subjected to two concentrated loads were made and tested under a static load with different arch lengths (1180 - 600 mm) but, with the same volume of concrete and amount of steel reinforcement. The depth of members is reduced at the central length according to the area and span of the arch, but the total depth at beam end equal (250 mm). Also, a total length ( $L_t$ ) of 1500 mm, the effective span ( $L$ ) was 1350 mm, the width ( $b$ ) for all beams was 150 mm, and the shear span ( $a$ ) was 450 mm as shown in Fig. 2.

According to ACI 318 requirements and the design method approved in the book of Thandavamoorthy, T.S., (2011)[1]; RC beams were designed. All beam specimens were tested under static two concentrated point loads. The two-hinged beam is a statically indeterminate structure to the first degree. Therefore, the Gaussian Quadrature method was used to perform numerical integration to obtain the horizontal thrust for non-prismatic members by using the strain energy stored in the hinged-hinged beam during deformation.

As longitudinal tension reinforcement, 2Ø12 mm deformed bars were available, and each

end steel bar had a 90° hook (12 times bar diameter) to provide sufficient anchorage. In addition, 2Ø10 mm was provided as longitudinal compression reinforcement. For shear reinforcement, it used Ø6 mm closed stirrups spaced at 90 mm c/c between two-point load and 85 mm c/c between support and load to prevent shear failure.

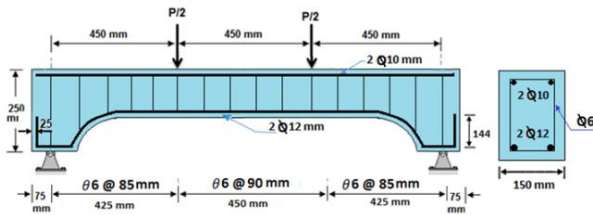


Fig. 2. Loading, reinforcement details and geometry of beams.

Tests on all beam specimens were conducted using two concentrated static point loads. The rigid steel roller with a 30 mm diameter welded by four 8 mm diameter bars used to its two sides to create a hinged supported condition. Between the concrete and steel hinge is a bearing plate made of steel that is (150 × 100 × 20) mm to prevent local failure at the loading and supporting points. The clear distance between these steel supporting is 1350 mm. As indicated in Fig. 3, the concentrated force is applied to the test specimen using a hydraulic jack of the testing apparatus with capacity of (1000) kN.

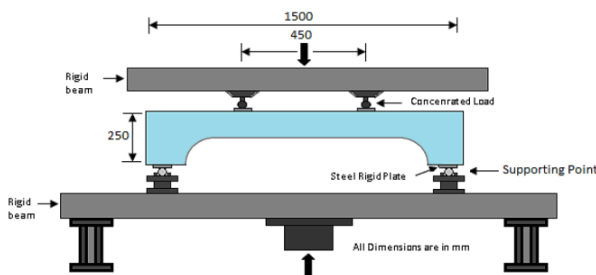


Fig. 3. Loading system for beam under concentrated loads.

Use equation (1) to achieve the same volume of concrete and steel reinforcement amount in beam, all specimens have the same area of the arch.

$V_{\text{beam}} = \text{width of beam} \times [\text{Total Area of beam-arch Area}]$

$$V_{\text{beam}} = 0.15 \times [1.5 \times 0.25 \text{-arch Area}]$$

Assume, arch Area = 0.06 m<sup>2</sup> (constant)

Where:  $V_{\text{beam}}$ : Volume of beam

A spanning member consists of a straight line and is usually cut into hollow curves at their ends. A radius corner arch is a simple yet elegant rounding of the corners of an opening. This arch has low header heights and larger openings. The radius corner arch gives the added benefit of a beautiful radius corner while allowing one to maintain the original header height as shown in Fig. 4. Equation (2) and (3) used to determine the dimensions of the radius corner arch.

$$A_{\text{arch}} = 2 \times \frac{\pi}{4} \cdot y_c^2 + y_c(L_c - 2y_c) \tag{1}$$

$$\text{but } A_{\text{arch}} = 0.06 \text{ m}^2$$

$$A_{\text{arch}} = 2 \times \frac{\pi}{4} \cdot y_c^2 + y_c(L_c - 2y_c) \tag{2}$$

$$0.06 = \frac{\pi}{2} \cdot y_c^2 + L_c \times y_c - 2y_c^2$$

$$y_c = \frac{2L_c \pm \sqrt{4L_c^2 - 4 \times 0.12(4 - \pi)}}{2(4 - \pi)}$$

Simplify more:

$$\therefore y_c = \frac{L_c \pm \sqrt{L_c^2 - 0.12(4 - \pi)}}{(4 - \pi)} \tag{3}$$

Where:  $A_{\text{arch}}$ : Area of the arch,  $y_c$ : Height of arch, and  $L_c$ : Span of the arch.

This arch has a quadrant of the circle at two ends with a radius equal to the height of the arch as well as a straight line in the middle. The arch height depends on the span of the arch to get the same area of the arch. Table 1 and Fig. 5 show the detail of beams with different arch spans (1180 - 600) mm.

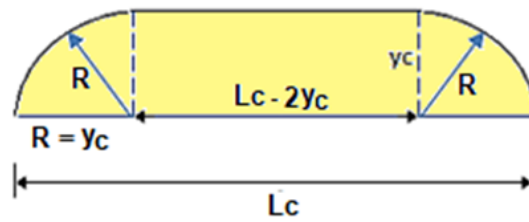


Fig. 4. Radius corner arch geometry.

Table 1. Information on tested beams.

Beam	$L_c$ (m)	$L_c/L$ ratio	$h$ (m)	$y_c$ (m)	$A_{\text{arch}}$ (m <sup>2</sup> )
R1	1.180	0.87	0.198	0.052	0.06
R2	0.900	0.67	0.180	0.070	0.06
R3	0.740	0.55	0.165	0.085	0.06
R4	0.600	0.44	0.142	0.108	0.06

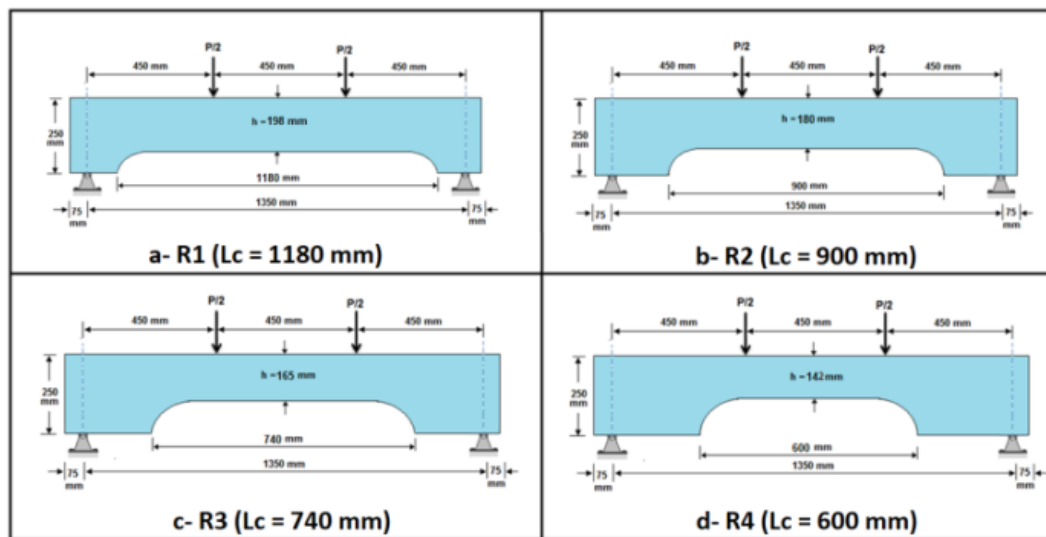


Fig. 5. Geometry and scheme loading of specimens of radius corner arch.

## 2.2. Material properties

the production of HSC are chosen based on good quality control, and suitable materials according The materials used in to ACI committee 363R, 2010[17] requirements. Ordinary Portland Cement called KAR Cement was used in this study. Fine aggregate with (2.94) fineness modulus and (4.75 mm) maximum size from Al-Akhaidur region in Iraq and coarse aggregate with 19 mm maximum size selected from Al-Nebai region were used. Also, the SikaViscocrete-5930 superplasticizers and Silica fume are required to produce (HSC) used to obtain high workability.

## 2.3. Procedure of the experimental work

The concrete mix for cementitious material, sand, gravel, and water cementitious ratio was by weight at 1:1.25:2.03:0.31 respectively, performed according to ACI committee 211.4R,1998[18] and according to previous researchers with a few changes to select the mix proportion for high strength concrete used in preparing the reinforced concrete beams to obtain cylinder strength of 50 MPa at 28 days. The internal dimensions of the beam molds were 1500 mm length, 150 mm width, and different depth along beam length. To ensure a clear appearance of crack growth during testing, the beam specimens were painted with white emulsion after 28 days of curing, see

Fig. 6. To obtain the mechanical properties of concrete, the average of three specimens for each compressive strength (cubes 150 mm<sup>3</sup>), tensile strength (cylinder 200 ×100) mm, and Rupture Modulus test (prisms (100×100×400) mm) were tested.



Fig. 6. Casting and curing process of beams.

### 3. Result of experimental work

#### 3.1. Material properties

The cubes, cylinders, and prisms were taken out of the water basin within 28 days of

casting by the standard specifications. Table 2 shows results of compressive, tensile strength, and rupture modulus for all beams.

Table 2. Mechanical properties values for beams.

Beam	Tensile Strength MPa		Compressive Strength MPa		Modulus of Elasticity** (E <sub>c</sub> ) GPa
	f <sub>sp</sub>	f <sub>r</sub>	Cube (f <sub>cu</sub> )	Cylinder (f <sub>c</sub> ) *	
R1	4.79	5.67	65.54	52.43	30.94
R2	4.75	6.11	68.21	54.57	31.43
R3	4.38	5.85	68.23	54.58	31.43
R4	4.69	5.66	67.87	54.30	31.36

\*f<sub>c</sub>' = 0.8f<sub>cu</sub>, \*\*ACI 363R-97[17] (E<sub>c</sub>=3320 √f<sub>c</sub>' +6900)

#### 3.2. Crack pattern and ultimate load

The first cracking load (P<sub>cr</sub>) which was obtained from experiments is presented in Table 3. Flexural, flexural shear (diagonal), and shear cracks developed during testing. Flexural cracks were noted firstly in all beams but in different locations. As loading continued, diagonal and shear cracks were observed.

Table 3. Experimental results for specimens.

Sample	First Cracking Load		Maximum load		Service Load [50]		
	Location	P <sub>cr</sub> (kN)	P <sub>u</sub> (kN)	Δu mm	P <sub>s</sub> (kN) 65%P <sub>u</sub>	Δs mm	W <sub>s</sub> mm
R1	20 cm from mid-span	30	93.41	10.24	60.72	4.29	0.58
R2	16.8 cm from mid-span	45	113.66	15.88	73.88	4.76	0.25
R3	11.3 cm from mid-span	35	105.43	14.18	68.53	4.58	0.75
R4	7 cm from mid-span	27	59.33	9.70	38.56	2.63	0.36

Δ<sub>all</sub> = L/240 = 5.625 mm according to ACI-Code 318-11 [19].

In general, the highest first cracking load is 45 kN of beam R2 which has the arch length to beam span ratio of (0.67). Also, it was found that the mid-span deflection at service load is lower than allowable deflection (L/240) according to ACI-Code 318-11[19] for all beams. The cracks pattern behavior of these specimens is discussed in the following:

#### 3.3. Load-deflection curves

Fig. 11. shows load-deflection curves for all specimens in different locations. As expected, with each increase in length of span gives better behavior, except for R1. It can be noticed that the stiffness and ultimate load of beam R2 are more than other beams.

The failure type, ultimate load, and deflection at midspan, under point load, and at the starting point of the arch are shown in Table 4.

According to the type of failure, it can be noted that the mode of failure for all beams failed in shear. Generally, the ultimate load ranged from (59.33 – 113.66) kN.

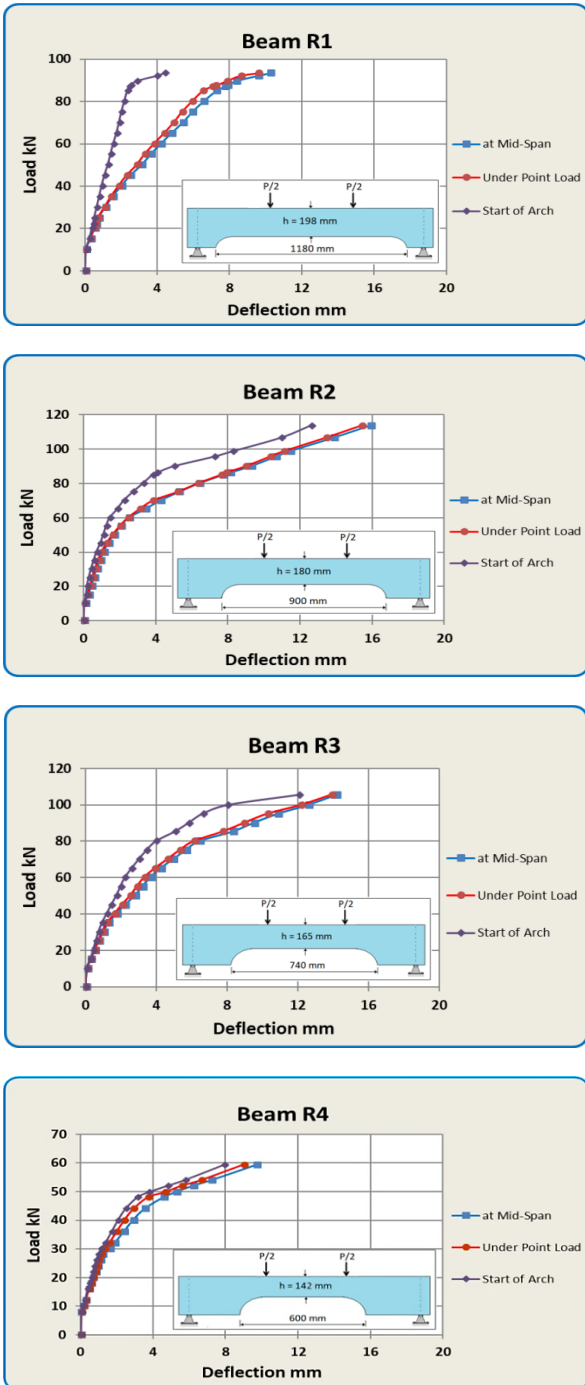


Fig. 11. Load deflection curves of beams with radius corner arch.

Fig. 12. shows load-deflection curves for all beams R1, R2, R3, and R4 at mid-span; it was noted that beam (R2) has more deflection and stiffness than other beams.

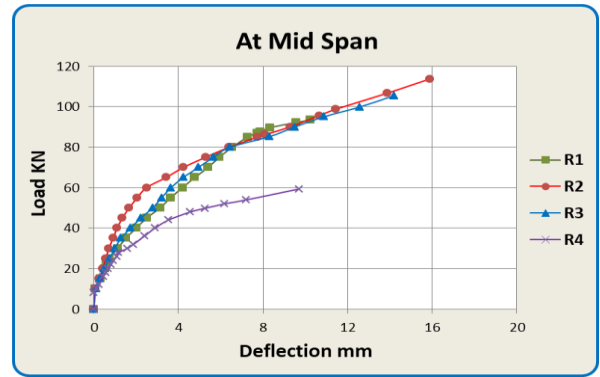


Fig. 12. Comparison of load - deflection curves for all beams at mid span.

### 3.4. Crack width

When the tensile strength reaches the concrete tensile stress, Cracking occurs in a beam. At each load of 10 kN, the max. crack width for all specimens was recorded by using the crack meter device as shown in Fig. 13. During recording the width of the crack for beams with the radius corner arch, the crack at the mid-span region did not increase in width but the inclined crack between the beginning of the arch and point load increased in width.

In the current study, it was found that the maximum crack width at the service load exceeded the allowable crack width for beams R1 and R3, see Table 3. The allowable crack widths in structures are highly variable. In ACI 318-11[19], that was based on empirical equations using a maximum crack width of 0.016 in (0.4 mm)[17].

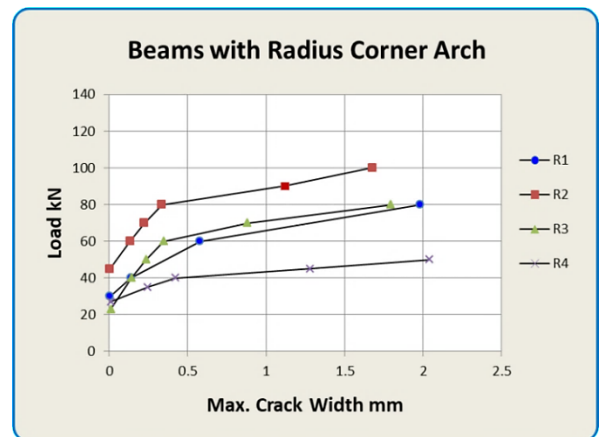


Fig. 13. The relationship between the max. crack width and load.

**Table 4.** Failure type, ultimate load and deflections for beams.

Sample	Ultimate Load			Deflection $\Delta u$ (mm)		
	Pu (kN)	% decrease in Ultimate load	Failure Mode	mid-span	At point load	Start of arch
R1	93.41	-----	Shear failure	10.24	9.57	4.93
R2	113.66	-21.68	Shear failure	15.88	15.4	12.59
R3	105.43	-12.87	Shear failure	14.18	13.88	12.05
R4	59.33	36.48	Shear failure	9.70	8.97	7.92

### 3.5. Deflected shape

Due to the symmetry of the tested beam models in both loading and geometry, one-half were used to distribute three dial gauges in the bottom face at (mid-span, point load, and starting of the arch) for measuring beam deflection. The deflection values were used to plot the deflected shape by using different values of load (each 20% of the ultimate load) by repeating the results of one side of beam through the central point to the other side along the symmetry axis. It was found that maximum deflection value at failure for all beams increased with increased length of the arch, except the beam at the length of 1180 mm excluded from this base, see Fig. 14.

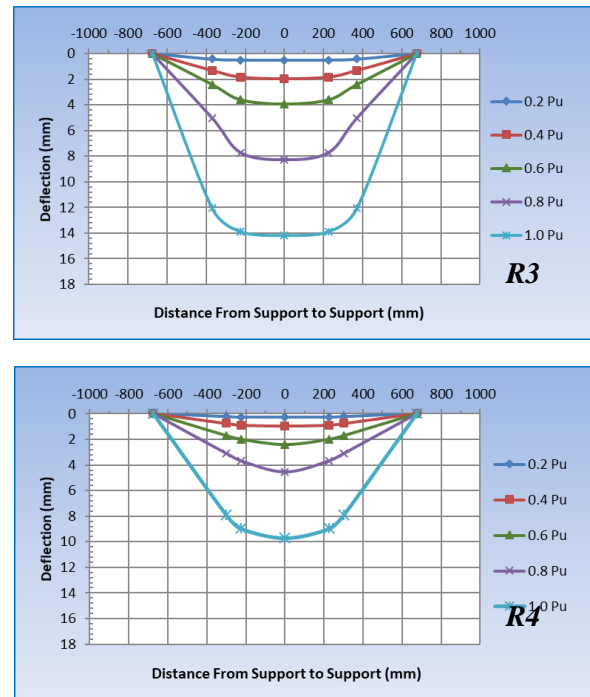
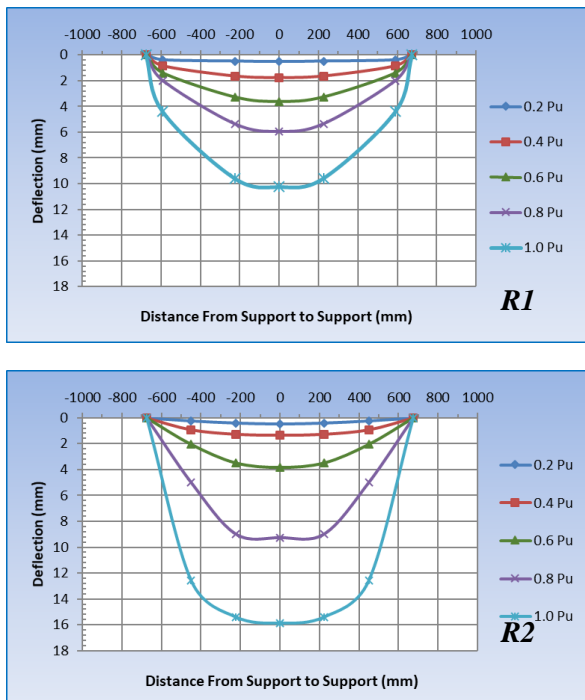


**Fig. 14.** Deflected shape of beams with radius corner arch.

Fig. 15. shows the comparison of the deflected shape for all beams at failure load.

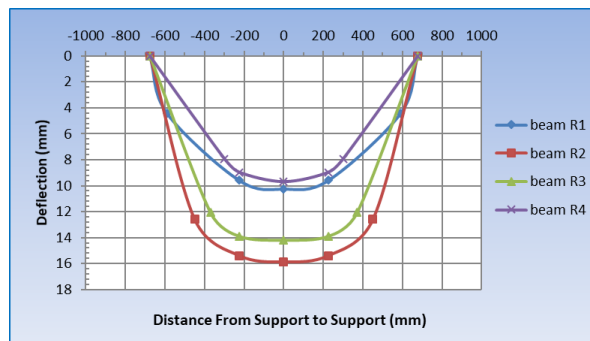


**Fig. 15.** Deflected shape at failure for all beams.

### 3.6. Effect ratio of arch length / span beam on behavior of beam

The arch length/beam span ratio has a major effect on the behavior of the beam with arched



bottom because it directly affects the ultimate capacity of the beams. The relation between the ultimate load and arch length / beam span ratio was described in Fig.16 which explains that the optimal ratio of the beam with radius corner arch is about (0.62).

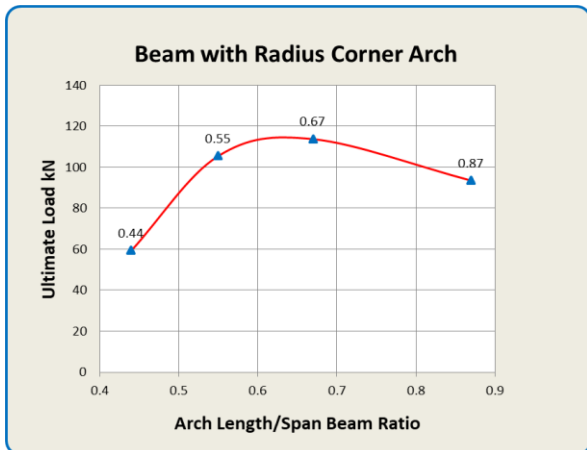


Fig. 16. The relationship between ultimate load and arch length / beam span ratio.

### 3.2.1. Beam R1 (arch length to beam span ratio ( $L_c/L = 0.87$ ))

At an applied load of (30 kN), the first crack was observed at 20 cm from mid-span near point load. At load (49 kN), flexural-shear cracks were observed, then increased in width and depth of the crack. As the load increases to (80 kN), a shear crack formation generally starts from corner of the arch towards the point load. Finally, beam failure in shear due to crack grew rapidly from support toward point load at load (93.41 kN), see Fig. 7.



Fig. 7. Cracks pattern at failure for beam (R1).

### 3.2.2. Beam R2 (arch length to beam span ratio ( $L_c/L = 0.67$ ))

Fig. 8 shows the crack pattern of the beam containing radius corner arch with arch length to beam span ratio ( $L_c/L = 0.67$ ). At an applied load of (45 kN), the first crack was noted at

16.8 cm from mid-span. As the load increased, it was observed the appearance of shear cracks formed. But at load (113.66 kN), sudden shear failure occurred. Here, beam R2 has a load carrying capacity more than R1 (with arch length to beam span ratio (0.87)) by about (21.68%).



Fig. 8. Cracks pattern at failure for beam (R2).

### 3.2.3. Beam R3 (arch length to beam span ratio ( $L_c/L = 0.55$ ))

In this specimen, it was observed that the first crack occurred between the two-point load region at 11.3 cm from mid-span when an applied load reached (35 kN). Flexural and shear cracks increased in width, number, and depth along the arch as the load increased. The failure was a fracture in the concrete cover followed by shear failure in concrete when the load reached an ultimate load of (105.43 kN) as shown in Fig. 9. Also, beam R3 has a load carrying capacity of more than specimen R1 about (12.87%) and less than specimen R2 about (7.24%).



Fig. 9. Cracks pattern at failure for beam (R3).

### 3.2.4. Beam R4 (arch length to beam span ratio ( $L_c/L = 0.44$ ))

The First crack of the beam (R4) was observed at 7 cm from mid-span when the load reached (27 kN). As loading continued, shear cracks formed between the beginning of the arch and the point load. When beam (R4) reached a load (59 kN), it occurred sudden loss of stiffness

and given a brittle behavior with shear failure mode. In addition, beam R4 has a load carrying capacity less than the beams (R1, R2, R3) by about (36.48%, 47.80%, and 43.73%) respectively, see Fig. 10.



Fig. 10. Cracks pattern at failure for beam (R4).

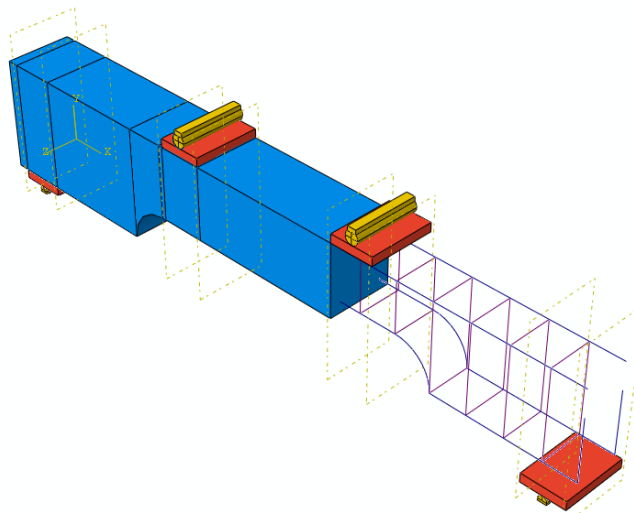


Fig. 17. Details modeling of beam models.

The behavior of RC material is nonlinear due to the sudden change for stiffness of the element which arises from yielding of tension reinforcement, crushing, cracking of the concrete, and plastic deformation of reinforcement and concrete. The concrete properties were defined depending on Concrete damaged plasticity models including compressive behavior, plasticity, and tensile behavior should be defined in ABAQUS.

The elastic behavior of concrete is defined by Young's modulus ( $E_c$ ) from ACI 363R (2010) [17] by  $E_c = 3320 \sqrt{f_c} + 6900$  and Poisson's ratio ( $\nu$ ) = 0.2. Table 5 presents the different variables used to represent the plastic properties of concrete.

## 4. Numerical study

### 4.1. Numerical study

The nonlinear finite element method (ABAQUS) was used to analyze a reinforced high-strength concrete beam containing an arch at the bottom face that provides a relatively acceptable numerical procedure. This work used three-dimensional solid elements for molded beams and assumed a full bond between concrete and steel. As stated before, a space eight-node element C3D8 was used for modeling the plate support, shaft, and concrete, and a space two-node truss element T3D2 was used for modeling reinforcement, see Fig.17.

Table 5. The different variables of the plastic properties of concrete.

Parameter	Magnitude	Depiction
$\psi$	31	The angle of dilation
$\epsilon$	0.1	Eccentricity
$f_{bo}/f_{co}$	1.16	The proportion between the primary compressive yield stress of equibiaxial and the initial compressive yield stress of uniaxial.
$K_c$	0.667	$K_c$ , the proportion of the tensile meridian and the second stress invariant
$\mu$	$10^{-7}$	Parameter of Viscosity

In the current study, the stress-strain relationship was adopted to represent the compressive behavior of the concrete, and this relationship depends mainly on the compressive strength of the concrete as shown in Fig. 18.

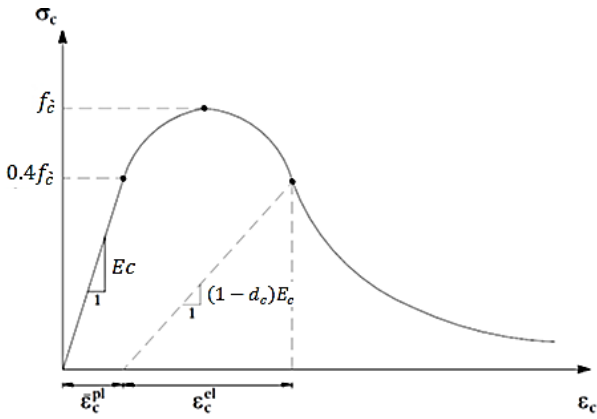


**Fig. 18.** Uniaxial compressive behavior of high strength concrete[20].

To represent the compressive and tensile behavior of concrete, we must rely on equations that have been derived from previous studies, as follows:

$$\sigma_c = f_c [2x - x^2] \quad (4)$$

Where:

$\sigma_c$ : the compressive stress of concrete,  $f_c$ : the compressive cylinder strength of concrete,  $x = \frac{\varepsilon_c}{\varepsilon_{co}}$ : the normalized strain,  $\varepsilon_c$  is the strain at any point,  $\varepsilon_{co} = 2f_c/E_c$  is the strain at peak stress[21]

$$\therefore \sigma_c = f_c \left[ 2 \left( \frac{\varepsilon_c}{\varepsilon_{co}} \right) - \left( \frac{\varepsilon_c}{\varepsilon_{co}} \right)^2 \right]$$

Plastic strain  $\varepsilon_{pl}$  at each point can be calculated according to Eq. (5),

$$\varepsilon_{pl} = \varepsilon_c - \frac{\sigma_c}{E_c} \quad (5)$$

Where:

$E_c$  is young's modulus of concrete.

To define the properties of steel bars, it is necessary to enter parameters related to their elastic and plastic behavior. The elastic behavior of steel bars should be determined by a linear elastic model in ABAQUS with Poisson's ratio ( $\nu$ ) and specifying Young's modulus ( $E_s$ ) of which typical values are 0.3 and 200 GPa, respectively. Plastic behavior represented by plastic strain and corresponding yield stress and is defined from experimental test.

#### 4.2. Numerical results

By using the ABAQUS computer program, the accuracy and validity of the adopted FE models are verified by evaluating all members experimentally tested in this study. The comparison between experimental and numerical load-deflection curves for beams with radius corner arch exhibited that the FE result is more rigid in the loading stages than the actual beam, see Fig. 19. But beam R2 at the first stage of loading has an experimental curve higher than the numerical curve until load (71 kN).

The load-deflection curves in the figures for each beam indicate how stiffer the F.E. results are than the actual beam. It differs because the F.E. does not consider the influence of micro-cracks, which are caused by drying shrinkage and handling and could decrease the stiffness of the actual beam. Concrete is a heterogeneous material, contrary to what the F.E. studies suggest. Additionally, in FE analysis, a perfect bond between the concrete and reinforcing bars is considered. However, in the actual beam, the above assumption could not be true. As a result, the overall stiffness of the beam could be less than predicted by F.E. studies.

Deflected shapes at failure load were taken as another test to confirm the application of the suggested numerical model. The deflected shape of beams at failure is shown in Fig. 20.

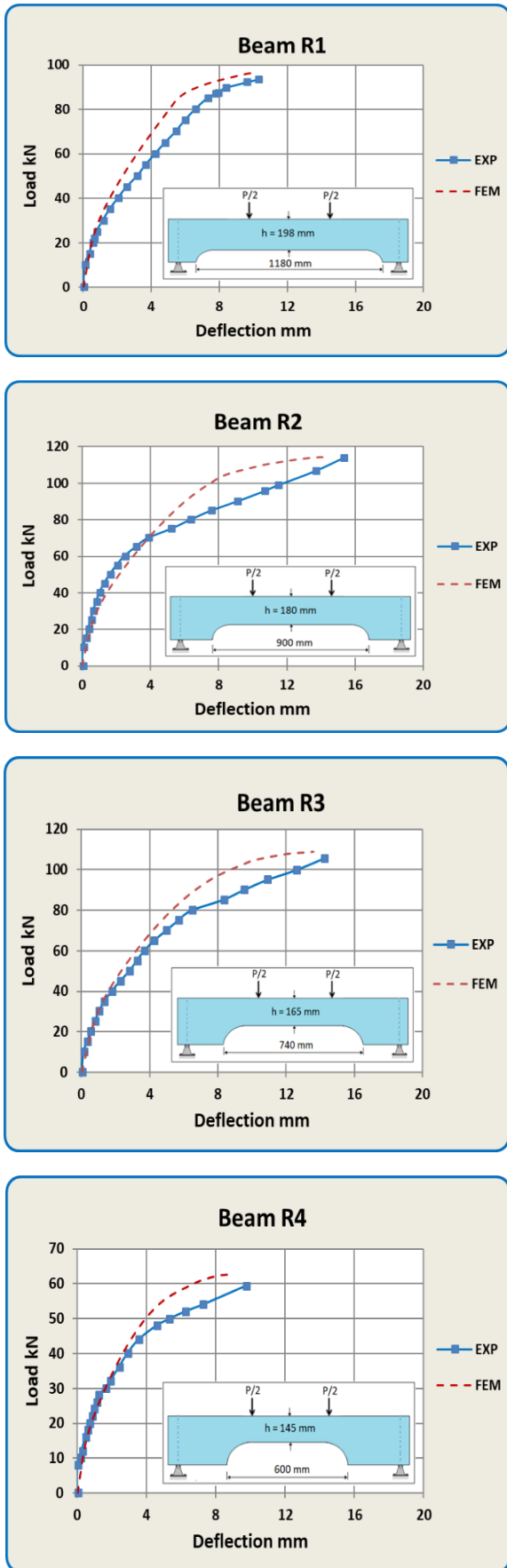


Fig. 19. Load-deflection curve for all beams.

From the results, it was found that the average difference ratio  $\frac{P_{cr)FEM}}{P_{cr)Exp}$  about (10.5%), meaning that the first numerical cracking load is less than the experimental data. Also, Fig. 21 illustrates the location of the first crack in this group at the beginning of the arch.

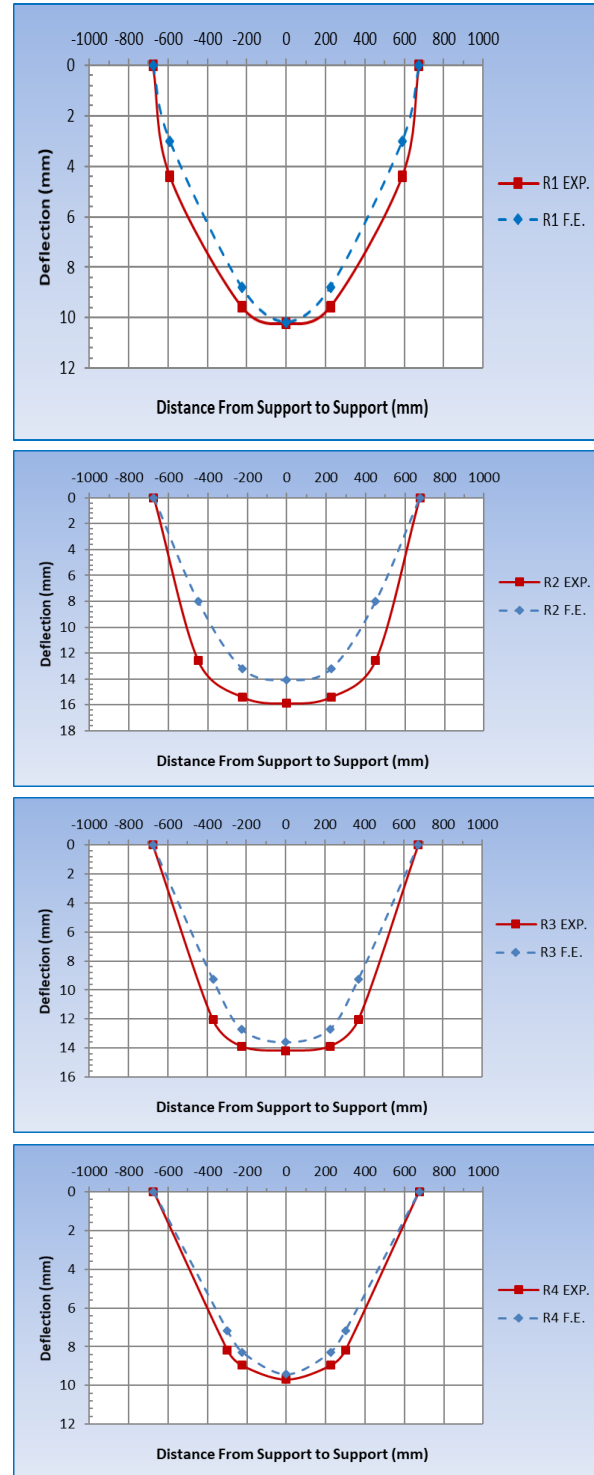
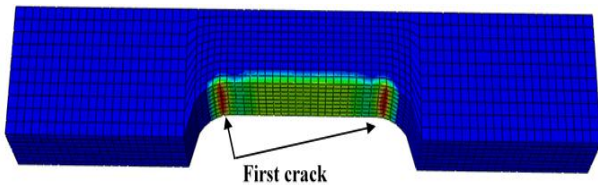


Fig. 20. Comparison of deflected shape at failure for beams.



**Fig. 21.** First crack loading for beams with radius corner arch.

Also, by comparing the maximum load of the experimental and numerical work, it was

found that the average increase in the numerical load is (3.5 %) as listed in Table 6. Also, we can notice that the average difference of the deflection at service load was about (8) between numerical and experimental work, and this indicates that the FEM result gives good accuracy. The deformed shape of beams with radius corner arch at the ultimate load shows in Fig. 22.

**Table 6.** Comparison between FEM and experimental result for all beams.

Beam Name	Cracking Load			Maximum Load (kN)			Deflection Δs (mm)		
	$P_{cr)Exp}$	$P_{cr)FEM}$	$\frac{P_{cr)FEM}}{P_{cr)Exp}$	$P_{u)Exp}$	$P_{u)FEM}$	$\frac{P_{u)FEM}}{P_{u)Exp}$	$\Delta_s)_{Exp}$	$\Delta_s)_{FEM}$	$\frac{\Delta_s)_{FEM}}{\Delta_s)_{Exp}}$
R1	30	26.5	0.88	93.41	96.91	1.04	4.29	3.44	0.80
R2	45	37.1	0.82	113.66	114.28	1.01	4.76	4.28	0.90
R3	35	31.25	0.89	105.43	108.8	1.03	4.58	4.33	0.95
R4	27	26.875	0.99	59.33	62.89	1.06	2.63	2.71	1.03
Av.			0.895			1.035			0.92

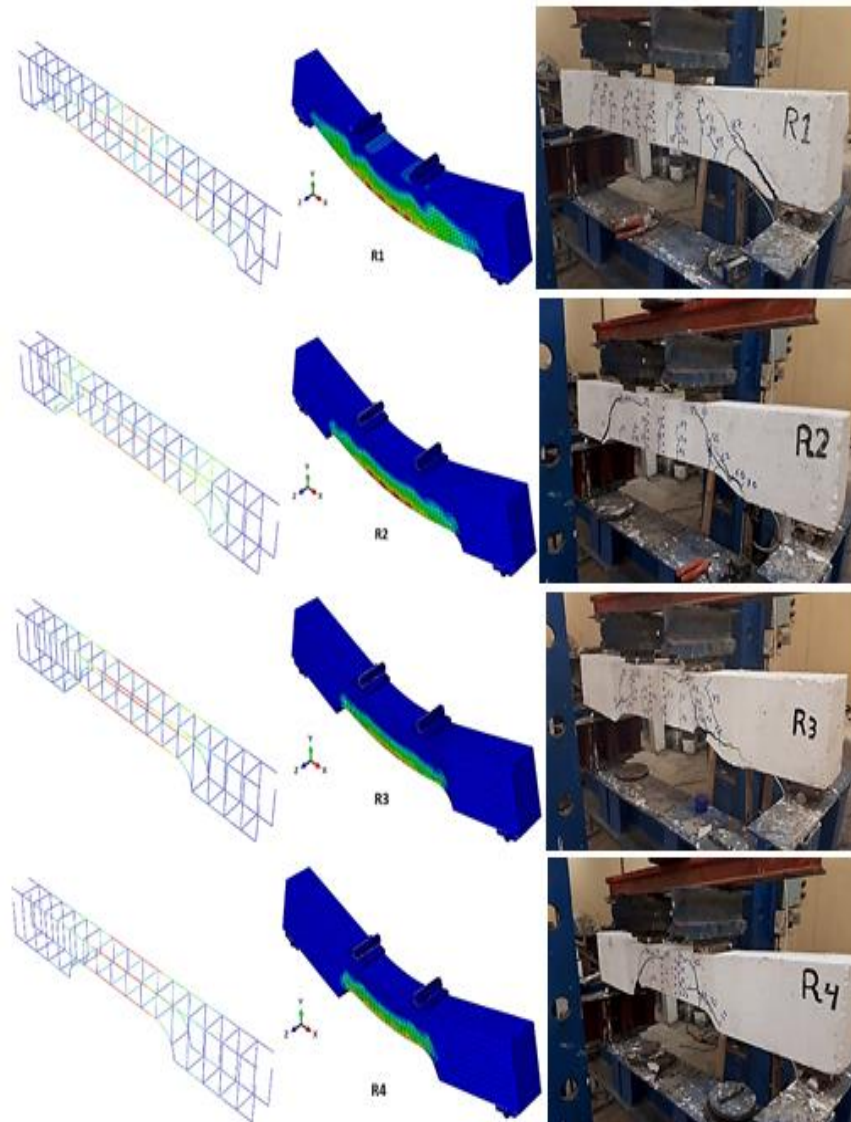


**Fig. 22.** Deformed shape for beams with radius corner arch at ultimate load.

## 5. Conclusions

Depending on the results of experimental work and finite element analysis by ABAQUS (Version 6, copyright 2014) Program for the two hinged beams with arched bottom under static loading, comparing the load-deflection behavior, cracks width, and mode of failure. The important conclusions obtained from the study are:

1. The optimal arch length/beam span ratio is 0.62 for beams with radius corner arch to get on best loading capacity. Also, all beams with radius corner arch failed due to shear effect.
2. The mid-span deflection at service load was less than the allowable deflection ( $L/180$ ) according to ACI-Code 318-11 for all tested types of beams with radius corner arch.
3. The first crack in all beams with radius corner arch were the flexural crack, but in variable locations. With increasing loading, crack width decreases with increasing arch length.
4. The FEM model gives good accuracy and seems efficient through comparison between the FEM and the experimental results in deflection where the average difference of the deflection in service load was less than 8% for all analyzed beams with radius corner arch. Also, the average increase in the ultimate numerical load for all beams with radius corner arch was about 3.5% when compared with the ultimate experimental load.

## Funding

No funding was received for this project.

## Conflict of interest

The authors certify that they have NO affiliations with or involvement in any organization or entity with any financial interest.

## Authors contribution statement

**Maryam H. Naser:** Conceptualization; Data curation; Formal analysis; Software and Writing – original draft.

**Fatimah H. Naser:** Investigation; Methodology; Project administration; Resources; Validation; Visualization; Writing – original draft; Writingreview & editing.

**Ali Hameed Naser Almamoori:** Data curation; Investigation; Methodology; Project administration; Supervision; Validation; Visualization and Writing – original draft.

**Mohammed L. Hussien:** Data curation, Investigation, Writing - review & editing of English language and grammar.

## References

- [1] Book: Thandavamoorthy T.S. “ Structural Analysis ” Oxford university press, first edition published in 2011 2011:2011.
- [2] Godínez-Domínguez EA, Tena-Colunga A, Juárez-Luna G. Nonlinear finite element modeling of reinforced concrete haunched beams designed to develop a shear failure. *Eng Struct* 2015;105:99–122.
- [3] Altaie E, Al-Ansari N, Knutsson S. Materials and the Style of Buildings used in Iraq during the Islamic period. *J Earth Sci Geotech Eng* 2012;2:69–97.
- [4] Alas RA. Computer program for the analysis of non-prismatic beams 1989.
- [5] Kaveh A, Mottaghi L, Izadifard RA. Sustainable design of reinforced concrete frames with non-prismatic beams. *Eng Comput* 2022;38:69–86. <https://doi.org/10.1007/s00366-020-01045-4>.
- [6] Archundia-Aranda HI, Tena-Colunga A, Grande-Vega A. Behavior of reinforced concrete haunched beams subjected to cyclic shear loading. *Eng Struct* 2013;49:27–42.
- [7] Luévanos-Rojas A. Mechanical elements of rectangular nonprismatic members for symmetrical parabolic haunches subjected to a uniformly distributed load. *J Archit Eng Technol* 2013;2:1–8.

- [8] Nabbat RA. Flexural and Shear Behavior of Non-Prismatic Reinforced High Strength Concrete Beams with Openings and Strengthened with CFPR Products 2015.
- [9] Jolly A, Vijayan V. Structural behaviour of reinforced concrete haunched beam: A study on ANSYS and ETABS. *Int J Innov Sci Eng Technol* 2016;3:495–500.
- [10] Naser MH, Falah MW, Hafedh AA, Naser FH. Parametric analysis and finite element modelling for shear behavior of positive haunched RC beams. *AIP Conf Proc* 2021;2404. <https://doi.org/10.1063/5.0069066>.
- [11] Elkersh IH, Lotfy E, Abd Ellatif E, Aboshosha MR. Flexural behavior of reinforced concrete beams with arched openings. *IOSR J Mech Civ Eng* 2020;17:25–36.
- [12] Sfakianakis MG, Fardis MN. Nonlinear finite element for modeling reinforced concrete columns in three-dimensional dynamic analysis. *Comput Struct* 1991;40:1405–19.
- [13] Al-Thabthawee DW. Nonlinear Analysis for Behavior of RC Arch Beams with Opening 2012.
- [14] Hamza BH. Behavior of RC Curved Beams with Openings and Strengthened by CFRP Laminates 2013.
- [15] Ali YA, Kadhum MJ. Nonlinear Analysis for behavior of Hollow Box Reinforced Concrete Arch Beams with Transverse Openings. *Nonlinear Anal* 2015;7.
- [16] Rad MM, Ibrahim SK, Lógó J. Limit design of reinforced concrete haunched beams by the control of the residual plastic deformation. *Structures*, vol. 39, Elsevier; 2022, p. 987–96.
- [17] Institute) ACI (American C. Report on high-strength concrete 2010.
- [18] ACI Committee 211. ACI 211.4R-93 Guide for Selecting Proportions for High-Strength Concrete with Portland Cement and Fly Ash. *Man Concr Pract* 1998;93:13.
- [19] Standard AA. Building code requirements for structural concrete (ACI 318-11). *Am. Concr. Inst.*, 2011.
- [20] Ahmed A. Modeling of a reinforced concrete beam subjected to impact vibration using ABAQUS. *Int J Civ Struct Eng* 2014;4:227–36.
- [21] Nilforoush R, Esfahani MS. Numerical Evaluation of Structural Behavior of the Simply Supported FRP-RC Beams. *Kungl. Tekniska Högskolan*; 2012.